De Gruyter Brill
Paradigm
ISSN 1335-8871

MEASUREMENT SCIENCE REVIEW

Journal homepage: https://reference-global.com/journal/MSR

Calibration of Thermodilatometer for Clay Ceramics and Uncertainty Analysis of RLTE and CLTE

Ján Ondruška[1*], Štefan Csáki[1,2], Igor Štubňa[1], Marek Mánik[1], Anton Trník[1]

[1]*Department of Physics, Faculty of Natural Sciences and Informatics, Constantine the Philosopher University in Nitra, Trieda Andreja Hlinku 1, 94901, Nitra, Slovakia, jondruska@ukf.sk, scsaki@ukf.sk, igor.c.stubna@gmail.com, mmanik@ukf.sk, atrnik@ukf.sk*

[2]*Department of Horticultural Machinery, Faculty of Horticulture, Mendel University in Brno, Valtická 337, 69144, Brno, Czech Republic, stefan.csaki@mendelu.cz*

Abstract: The relative linear thermal expansion (RLTE) and coefficient of linear thermal expansion (CLTE) of a kaolinite-based clay sample were determined using a horizontal alumina push-rod dilatometer in the range 20 °C – 1100 °C. The dilatometer configuration is described along with potential sources of measurement uncertainty. An uncertainty analysis was performed, accounting for temperature-field homogeneity, specimen positioning, mechanical pressure on the sample, thermocouple ageing and corrosion, temperature-control stability, the linear variable differential transformer (LVDT) constant, and the precision of the LVDT output signal. Uncertainties associated with the used instruments were also considered. The summation of individual uncertainty components yields the expanded uncertainty for the thermodilatometric analysis. The uncertainty of RLTE is temperature-dependent, reaching a maximum of ~5.26 % at 800 °C, where the maximum scatter of RLTE was observed. When only ordinary thermal expansion occurs, the uncertainty of the RLTE is ~1 %, and the uncertainty of the CLTE is ~3 %.

Keywords: push-rod dilatometer, calibration of dilatometer, uncertainty analysis

1. INTRODUCTION

Solid materials, such as ceramics and their constituent minerals, exhibit thermal expansion upon heating. In specific instances, structural modifications, such as dehydroxylation in natural clays, occur during heating. These transformations are typically accompanied by significant variations in specific volume, which can be measured by the corresponding change in sample length. The measurement of its thermal dilatation during linear heating/cooling or isothermal heating, called thermodilatometric analysis (TDA), is an important tool for determining phase-transformation kinetics, sintering in ceramics, optimizing the firing regime, estimating mineral composition, and other applications [1]-[5].

The physical quantity characterizing thermal expansion is the coefficient of linear thermal expansion α (CLTE) derived from the relative linear thermal expansion (RLTE). Let a sample have an initial length l_0 at room temperature t_0. When the sample is heated, it expands to l_1 at t_1, and then to l_2 at t_2. The instantaneous CLTE within the temperature interval (t_1, t_2) at the mean temperature t_m is defined as [6]

$$\alpha(t_m) = \frac{1}{l_0}\frac{l_2 - l_1}{t_2 - t_1} = \frac{1}{l_0}\frac{\Delta l}{\Delta t}, \quad t_m = \frac{t_1 + t_2}{2}. \qquad (1)$$

The derivative defines the instantaneous CLTE $\mathrm{d}l/\mathrm{d}t$ at a single temperature. This represents the limiting case of (1) as t_1 and t_2 become very close to each other. The fundamental basis for determining the CLTE is the RLTE $\Delta l/l_0$; its derivative $\mathrm{d}(\Delta l/l_0)/\mathrm{d}t$ yields the CLTE.

A survey of dilatometric results obtained for fired ceramics indicates that $\Delta l/l_0 < 1$ % within the temperature interval of 20-1300 °C. During the sintering of the green sample, a significant contraction $\Delta l/l_0 > 12$ % can be observed in this temperature interval. In addition, certain phase changes are accompanied by large shrinkage, e.g., the intensive rebuilding of the crystal lattice during dehydroxylation and the formation of new phases at 950 °C in clay ceramics. Consequently, a large measurement range, rather than extreme sensitivity, is required for TDA of green clay ceramics. A resolution of 1×10^{-6} m is sufficient for most experimental investigations. A push-rod dilatometer with a linear variable differential transformer (LVDT) and alumina support elements (tube or rods) effectively fulfills these requirements.

A differential horizontal alumina dilatometer, designed and constructed in the authors' laboratory, was used to measure the thermal expansion of kaolinite- and illite-based samples, as well as ceramic components (quartz, feldspar,

DOI: 10.2478/msr-2026-0037
*Corresponding author: jondruska@ukf.sk (J. Ondruška)
© 2026 Institute of Measurement Science, SAS. This work is licensed under CC BY-NC-ND 4.0.

calcite, kaolin, and various clays) during heating from room temperature to 1250 °C [5]-[11].

The calibration of relative dilatometers is infrequently addressed in the research literature. Furthermore, the authors have not encountered studies that focus on uncertainty analysis of TDA results obtained during thermal treatment. The objective of the present study is to provide a detailed description of the dilatometer calibration and to estimate the measurement uncertainty associated with RLTE and CLTE.

2. DILATOMETER

The push-rod dilatometer uses a differential measurement technique to determine the relative displacement between the expansion of alumina carrier components (rods or tubes) with a known RLTE and that of a sample with unknown thermal expansion.

Different techniques for measuring the thermal expansion of solids are briefly reviewed in [1], [12]-[14]; however, no previously reported dilatometric cell design is identical to the configuration used in the present study. A similar construction was reported in [15], [16]. A dilatometric cell, as illustrated in Fig. 1 and Fig. 2, consists of four carrier alumina rods (⌀3.0 mm) secured to two duralumin holders, along with the push-rod and supporting rod.

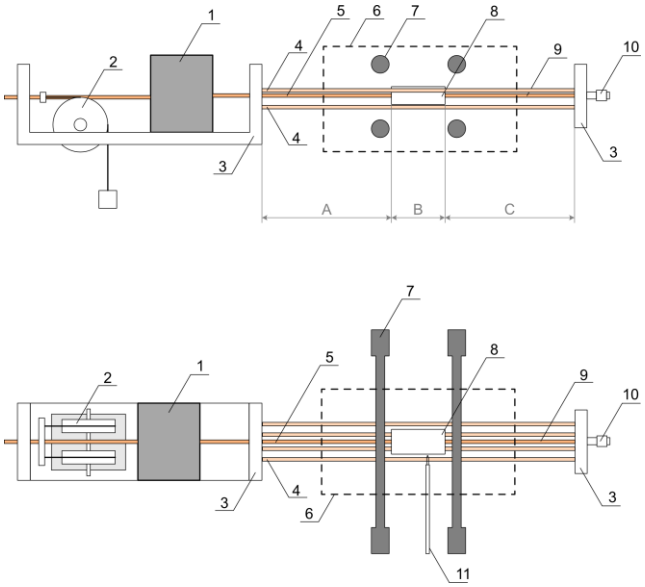

Fig. 1. Schematic diagram of the dilatometer: a) side view; b) top view. 1 – LVDT, 2 – pulley with load, 3 – holder, 4 – carrier alumina rods, 5 – push-rod, 6 – furnace, 7 – heating element, 8 – sample, 9 – supporting rod, 10 – micrometric zeroing screw, 11 – thermocouple.

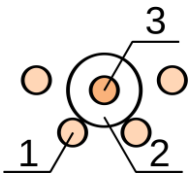

Fig. 2. Cross-section of the dilatometric cell. 1 – four carrier rods, 2 – sample, 3 – push-rod or supporting rod.

The LVDT (INPOS, ZPA Jinonice, Czech Republic) is fixed to one of the holders. The assembly features a lightweight design, with neither holder being rigidly fixed to the apparatus frame. The cell assembly passes freely through the furnace openings, which are insulated with ceramic fiber.

The push-rod is pressed against the sample with a weight to enable loading for dilatometry (e.g., compressive creep). The furnace is constructed from porous alumina bricks, and four silicon carbide (SiC) rods are used as heating elements. The operational temperature range of the dilatometer is 20 °C to 1250 °C under a static air atmosphere.

The central part of the dilatometric cell, containing the sample, is located within the furnace. A cross-sectional view of the dilatometric cell illustrating the spatial arrangement of the carrier rods, sample, and push-rod is presented in Fig. 2. The sample is placed between two rods: the push-rod and the stationary supporting rod, the latter being fixed to the second holder. The axial position of the push-rod, specimen, and supporting rod assembly is adjustable via a micrometric screw. The LVDT measures the displacement of the push-rod, Δd, which corresponds to the sample's relative longitudinal deformation. An Agilent 34972A DC multimeter measures analog voltage signals from both the LVDT and the thermocouple, then digitizes and stores them on a personal computer. Temperature expansion measurements are performed in adjustable steps ranging from 10 s to 3 min.

The furnace temperature is measured using a Pt-PtRh10 thermocouple placed near the sample. The temperature is controlled by a temperature programmer, Clasic Clare 4 (Czech Republic), operating independently of the PC. The multimeter performs internal cold junction compensation and voltage-to-temperature conversion for the Pt-PtRh10 thermocouple.

The presented design allows adjustment of the measurement cell for samples with dimensions ⌀5 × 25 mm up to ⌀10 × 70 mm. This flexibility enables the measurement of inhomogeneous materials that contain coarse grains or textured microstructure. The constant pressure of the push-rod on the sample is achieved by gravity acting on the weight. This further permits adjustment of the pressing force and monitoring of compression creep behavior.

The basic scheme of the dilatometer shown in Fig. 1 highlights that only differential expansion in section B contributes to the LVDT signal, as expansions in sections A and C are compensated. The LVDT measures $\Delta U = U - U_0$ voltage at elevated temperature t, resulting from the relative displacement of the push-rod, Δl, between the sample and alumina carrier rods, which expand in opposite directions. The initial voltage U_0 is adjusted at room temperature, assuming the linear relationship between Δl and ΔU, i.e. $\Delta l = k\Delta U$. The following expression holds for an ideal dilatometer:

$$k\Delta U = \Delta l_s - \Delta l_{ar}, \tag{2}$$

where Δl_s is the change in the length of the sample, Δl_{ar} is the change in the length of the carrier alumina rods at temperature t, and k is the experimentally determined LVDT constant.

The relative expansion of the alumina rod is known across the entire temperature range. By defining l_0 as the initial sample length, the RLTE of the sample is calculated using the known RLTE values of alumina $\Delta l_{ar}/l_0$ and the measured values of ΔU. The RLTE of the sample $\Delta l_s/l_0$ is then derived from (2) as follows:

$$\varepsilon = \frac{\Delta l_s}{l_0} = \frac{k\Delta U}{l_0} + \left(\frac{\Delta l_{ar}}{l_0} + \frac{\Delta l_{se}}{l_0}\right). \tag{3}$$

In (3), a term $\Delta l_{se}/l_0$ is incorporated to account for the contribution of systematic errors (e.g., zero drift) inherent to the real dilatometer. Once the RLTE of the sample is determined, CLTE over the temperature interval Δt can be calculated as

$$\alpha = \frac{\varepsilon}{\Delta t} = \frac{1}{l_0}\frac{\Delta l_s}{\Delta t}. \tag{4}$$

3. Calibration

Since the employed method is not absolute, the calibration of the dilatometer is necessary [6], [17]-[19]. Calibration was performed at a heating rate of 5 °C/min, a commonly used thermal regime in the authors' laboratory. For this purpose, a reference sample for dilatometry (⌀5 × 30.00 mm) of X10NiCrMoTiB 1515 steel, provided by the Physikalisch-Technische Bundesanstalt (National Metrology Institute), Berlin, was used. This material has been intensively studied in recent studies. Tabulated data from the round-robin test [20] were adopted as the reference dilatometric curve (Fig. 3), which the following linear function can express

$$\varepsilon_{ref} = \left(\frac{\Delta l}{l_0}\right)_{ref} = 2.01 \times 10^{-3} t - 8.09 \times 10^{-2}, \quad R^2 = 0.9994\,, \tag{5}$$

where t is in °C and ε_{ref} is in %.

As previously noted, the carrier rods compensate for the thermal expansion of the push-rod and the support rod when their temperatures are equal. In a real dilatometer, an additional small displacement of the push-rod arises from minor temperature differences among the dilatometer elements during heating. This undesirable displacement can be characterized by performing a TDA test using a sample from the alumina rod. The resulting data define the dilatometer's baseline for the specific thermal regime. The mean gradient of the baseline (Fig. 3) of the calibrated dilatometer was 2.62×10^{-7} 1/°C, which was below the maximum permissible limit of 3×10^{-7} 1/°C for a properly configured dilatometer [6]. To eliminate this error, the calibration using the reference sample must be performed [17].

The first stage of the calibration procedure involved the experimental determination of the LVDT constant, k, in (2) at room temperature. The value of k was obtained by measuring the output of the LVDT $\Delta U = U - U_0$ (U_0 denotes the initial voltage) and the displacement Δl of the push-rod controlled by a micrometric screw. The obtained LVDT constant $k = -1.907 \pm 0.004$ mm/V was used in subsequent analysis.

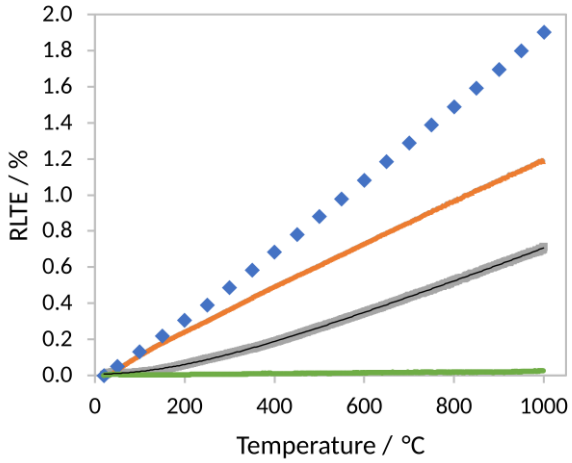

Fig. 3. Dilatometric reference line plotted from the tabulated values in [20] (♦), the mean value of the repeatedly measured reference sample (orange), correction function with error bars and mean value line (grey), and baseline (green).

The reference sample was measured 5 times at a heating rate of 5 °C/min. The experimental data obtained over the temperature range 20 °C – 1000 °C (Fig. 3) were used for calibration. The difference $\Delta\varepsilon(t)$ between the reference data $\varepsilon_{ref}(t)$ and the experimental data $\varepsilon_{exp}(t)$ must be added to the experimental data to obtain the reference values, i.e., $\varepsilon_{ref}(t) = \varepsilon_{exp}(t) + \Delta\varepsilon(t)$. This difference, $\Delta\varepsilon(t)$, is the correction function and corresponds to the term in parentheses in (3). The analytical expression of the correction function obtained via polynomial fitting is defined as

$$\varepsilon_{cor} = \left(\frac{\Delta l}{l_0}\right)_{cor} = -4.316 \times 10^{-10} t^3 + 9.893 \times 10^{-7} t^2 + 1.44 \times 10^{-4} t - 1.05 \times 10^{-3}, \quad R^2 = 0.9998, \tag{6}$$

where t is in °C and ε_{cor} is in %.

Equation (3) can be written using (6) as

$$\varepsilon = \frac{\Delta l_s}{l_0} = 100k\frac{\Delta U}{l_0} + (-4.316 \times 10^{-10} t_m^3 + 9.893 \times 10^{-7} t_m^2 + 1.44 \times 10^{-4} t_m - 1.05 \times 10^{-3}), \tag{7}$$

where ε is in %, l_0 in mm, $\Delta U = (U - U_0)$ in V, $t_m = (t_2 + t_1)/2$ in °C, and $k = -1.907$ mm/V. The temperatures t_1 and t_2 represent the most proximal values centered around ~800 °C.

In addition to mechanical calibration of the dilatometer, a temperature calibration should be performed if a high-precision TDA is required. The procedure involves heating a composite specimen consisting of thin metallic foils sandwiched between alumina segments. Upon reaching the melting point of the metallic standard, a distinct discontinuity is observed in the TDA curve. This technique enables the determination of the deviation between the actual specimen temperature and the recorded temperature [18], [21]. Given that the kinetic processes in ceramic specimens typically proceed gradually over extended temperature intervals, extreme temperature precision is not strictly required for these applications. A simple test based on the melting point

of aluminum (660.3 °C), the $\alpha \rightarrow \beta$ transition of quartz (573 °C), the $\alpha \rightarrow \beta$ transition of cristobalite (~220 °C), and the metakaolinite lattice collapse (~950 °C) confirmed that these transformations occur in the dilatometer close to their theoretical characteristic temperatures.

The sensitivity of the dilatometer, as determined by the minimum resolvable increment in the Δl_s record, is 6×10^{-8} m. The minimal resolvable increment Δl_s was determined from the smallest detectable change in the output voltage ΔU of the LVDT sensor, according to the relation $\Delta l_s = k\Delta U$, where k is the calibration constant of the sensor. This determination was performed at a slow heating rate of 2 °C/min to ensure stable signal conditions.

The correctness of the calibration was verified by TDA on a quartz monocrystal along its c-axis at a heating rate of 5 °C/min. The experimental results show very good agreement with the data reported in [22]-[26] from five independent sources, see Fig. 4.

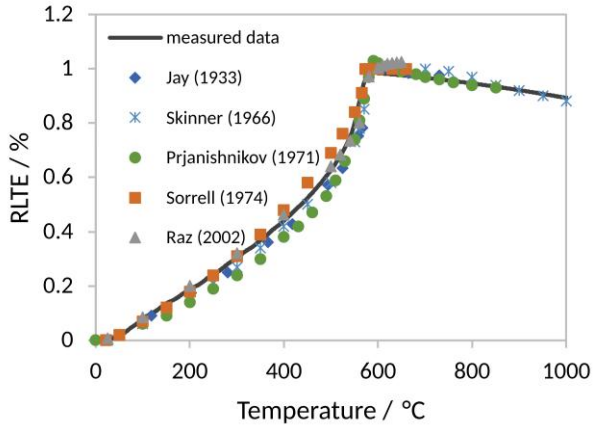

Fig. 4. Comparison of the RLTE of the quartz monocrystal along its c-axis [22]-[26] with the experimentally determined RLTE (solid line).

4. Uncertainty analysis of RLTE and CLTE

The standard wet-ceramic processing was used to prepare the samples: mineral powders were mixed with water to form a plastic ceramic mass. A plastic ceramic mixture consisting of kaolinite (50 wt.%), ground quartz (25 wt.%), and albite (25 wt.%), with particle sizes below 200 μm, was used to produce an extruded die-cast rod of ⌀8 × 200 mm. From this rod, samples of ⌀8 × 33 mm were cut, ensuring an identical microstructure across all specimens. After drying, the samples were subjected to TDA at a heating rate of 5 °C/min.

The data in Fig. 5 indicate the temporary scatter (650 °C – 1000 °C). Above 1000 °C, all RLTE curves converge again, and only minimal variation is observed. The temperature range in which the scatter appears corresponds to pronounced microstructural and structural changes caused by solid-state and liquid-phase sintering, as well as the collapse of metakaolinite. These processes inherently involve thermally driven structural rearrangements, making thermal randomness the most probable source of the observed scatter.

The uncertainty analysis was performed in two stages: a) for the RLTE of the unfired sample, b) for CLTE. Upon inspecting the TDA curve (Fig. 5), significant scatter in the measured values was observed at 800 °C; therefore, the uncertainty analysis focused on this temperature.

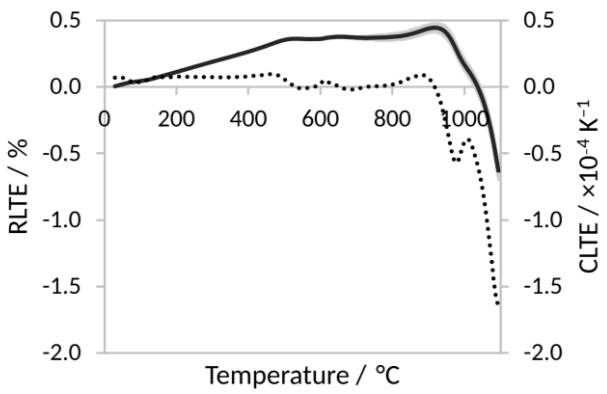

Fig. 5. Thermodilatometric analysis of a clay sample. The solid line represents RLTE (left axis), the mean of five measurements, with the gray band indicating the error bars. The dotted line is the corresponding CLTE (right axis), obtained as the temperature derivative of the RLTE. The extrema of the CLTE curve identify the temperatures of maximum intensity of the individual processes: release of physically bound water (20 °C → 300 °C), dehydroxylation (400 °C → 750 °C), sintering (above 700 °C), and the formation of new phases (above 900 °C).

According to [27], measurement uncertainty comprises components of two types, A and B. A-type uncertainties are evaluated through statistical analysis; the uncertainty of the measured quantity x_i is defined as

$$u_A(x) = \frac{s_i}{\sqrt{n}} = \sqrt{\frac{1}{n(n-1)} \sum_{i=1}^{n} (x_i - \bar{x})^2}, \tag{8}$$

where s_i denotes the standard deviation, n is the number of independent measurements, and $\bar{x}$ is the mean value.

Each dilatometric analysis assumes measuring the initial sample length l_0 at room temperature. According to [28], the length l_0 should be measured with a relative error $\Delta l/l_0 < 0.2$ %. The length of the sample l_0 was measured six times at room temperature, and the standard uncertainty of l_0 is 0.01 mm (see Table 1), or 3×10^{-4} (0.03 %), i.e., the requirement of [28] is fulfilled.

The sample used for the uncertainty analysis consisted of illitic clay. Upon heating, the clay sample undergoes irreversible processes, transforming the raw material into a sintered ceramic body. To determine Type A uncertainty, which is derived from repeated measurements, a series of identical samples must be used. Therefore, TDA of the clay sample was repeated 5 times, always with a fresh sample, see Fig. 5. The LVDT output voltage, U, at temperature t (closest to 800 °C) was recorded every 30 s, i.e., in $\Delta t = 2.5$ °C steps. The voltages U and U_0, as well as temperature t, were extracted from the protocol stored in the PC for each individual TDA.

The mean values of l_0, t, and ΔU, with their standard deviations and A-type standard uncertainties $u_A(x)$ are presented in Table 1.

Table 1. The mean value $\bar{x}$, standard deviation s, and standard uncertainty of the A-type $u_A(x_i)$.

	at 20 °C		at 800 °C	
	k / mm/V	l_0 / mm	t_m / °C	ΔU / V
$\bar{x}$	–1.907	32.23	797.6	0.025
s	0.004	0.025	2.07	0.004
$u_A(x)$	0.002	0.010	1.20	0.002

The sum of the A-type uncertainties, which follows from the directly measured quantities in (7), is

$$u_A(\varepsilon) = \sqrt{\begin{matrix} A^2(k)\,u_A^2(k) + A^2(l_0)\,u_A^2(l_0) + \\ +A^2(\Delta U)\,u_A^2(\Delta U) + A^2(t_m)\,u_A^2(t_m) \end{matrix}}, \quad (9)$$

where sensitivity coefficients $A(x_i)$ are partial derivatives of (7)

$$A(k) = \frac{\partial \varepsilon}{\partial k} = \frac{\Delta U}{l_0}, \qquad A(l_0) = \frac{\partial \varepsilon}{\partial l_0} = -k\frac{\Delta U}{l_0^2},$$

$$A(\Delta U) = \frac{\partial \varepsilon}{\partial (\Delta U)} = k\frac{1}{l_0},$$

$$A(t) = \frac{\partial \varepsilon}{\partial t_m} = -1.295 \times 10^{-9} t_m^2 + 1.977 \times 10^{-6} t_m + \\ +1.44 \times 10^{-4}.$$

The mean values from Table 1 were substituted into the sensitivity coefficients to obtain their numerical values (see Table 2).

The CLTE can be obtained via numerical differentiation of RLTE by dividing ε by a small temperature interval Δt, see (4). The sensitivity coefficients for CLTE are

$$A(\varepsilon) = \frac{\partial \alpha}{\partial \varepsilon} = \frac{1}{\Delta t}, \qquad A(\Delta t) = \frac{\partial \alpha}{\partial (\Delta t)} = -\frac{\varepsilon}{(\Delta t)^2}. \quad (10)$$

The ε for 800 °C is the mean value of the RLTE, and Δt = 2.5 °C was determined from the applied heating rate (5 °C/min) and the selected sampling interval (0.5 min).

The B-type uncertainties, $u_B(x_i)$, are evaluated from the manufacturer's specifications, calibration certificates, and expert knowledge. These uncertainties originate from various independent sources and represent systematic effects that cannot be treated statistically. For the digital and analog measuring devices used in this study, the B-type uncertainties are expressed as $u_B(x_i) = MAE/\sqrt{3}$ and $u_B(x_i) = r/\sqrt{12}$, where MAE is the maximum admissible error and r is the resolution of the instrument. Additional B-type uncertainties result from factors influencing the displacement of the push-rod, and each of these contributions must be evaluated individually.

The sum of the B-type uncertainties is given by the equation

$$u_B(\varepsilon) = \sqrt{\sum_{i=1}^{m} A^2(x_i) u_B^2(x_i)}, \quad (11)$$

where m is the number of sources of B-type uncertainties.

A. Sources of B-type uncertainties:

The LVDT constant

Using the constant k, the output voltage from the LVDT is converted into push-rod displacement: $\Delta l_s = k\Delta U$. The LVDT was calibrated using an analog micrometer with a resolution r = 0.01 mm; consequently, the standard uncertainty of the micrometer is $r/\sqrt{12} \approx 2.9 \times 10^{-3}$ mm, which is equal to $u_B(k)$, see line 9 in Table 2.

The sample position

The sample location within the dilatometric cell is strictly defined by its construction; consequently, it does not influence the value of $\Delta l_s/l_0$. The sample, push-rod, and supporting rod may not be perfectly centered, which could introduce an estimated shift of 2 × 10^{-3} mm.

Mechanical pressure on the sample

Reliable mechanical contact between the push-rod, supporting rod, and the sample is maintained by a weight. As a result, a compressive force causes their deformation. Taking into account a compressive force F = 0.1 N, the dimensions of the rods and ceramic sample, as well as the temperature dependence of their Young's moduli, the total deformation is estimated at ~2.5 × 10^{-5} mm at temperatures below 1000 °C.

The thermocouple aging and corrosion

Exposed Pt-PtRh10 (type S) thermocouples undergo corrosion and aging during service. The aging is minimal at temperatures below 1400 °C, and the influence of corrosion (due to silicon) is low for wires thicker than 0.3 mm. Consequently, the thermocouple was considered a stable sensor with invariant properties.

Note: in the subsequent sections, the estimated temperature deviation Δt was converted into the push-rod displacement Δl for l_0 = 32.23 mm and a CLTE of the sample material $\alpha = 3.12 \times 10^{-6}$ 1/K around 800 °C:
$\Delta l = l_0 \alpha \Delta t = 1.00 \times 10^{-4}\ \Delta t$.

The thermocouple and temperature control

A typical accuracy of a Pt-PtRh10 thermocouple is within ~1 % of the measured temperature, i.e., ~8.0 °C at 800 °C. This temperature deviation induces a push-rod displacement of ~8.0 × 10^{-3} mm due to the sample's thermal expansion.

The temperature controller Clasic Clare 4 (Czech Republic) is used to regulate the thermal regime (heating, cooling, or isothermal) within the furnace. According to the manufacturer's specifications, the temperature error is ~1 °C at 800 °C, and the long-term stability is 0.3 °C when the room temperature changes by 10 °C. Consequently, the temperature controller can introduce additional sample expansion ~1.8 × 10^{-3} mm.

The compensation leads connect the thermocouple wires to the input of an Agilent 34972A multimeter, which performs cold-junction compensation and converts the thermoelectric voltage into temperature. The error associated with cold junction compensation is negligible, at less than 0.3 °C. Combined with the thermocouple error, the cumulative temperature error is ~1.5 °C. This can cause a small shift in the push-rod of ~3 × 10^{-4} mm.

The influence of temperature field inhomogeneity

When the temperature is not uniformly distributed throughout the sample volume, the sample's properties depend on position. Consequently, a homogeneous temperature field is required in the region surrounding the sample. Since the carrier rods do not shield the sample from the heating elements, the measuring cell temperature is distributed uniformly. The internal dimensions of the furnace are 100 × 70 × 70 mm. The thermal field in the central region of the dilatometric cell was measured at constant temperatures of 900 °C and 1150 °C. It was found that temperature deviations between the sample center and its ends were less than 3 °C at 1150 °C, which falls within the permitted interval specified by [28]. For Δt = 3 °C, the uncertainty is 6.0 × 10^{-4} mm.

The combined uncertainty of the linear thermal expansion is defined as the square root of the sum of the squared uncertainty components listed in Table 2, lines 6 and 17

$$u_C(\varepsilon) = \sqrt{u_A^2(\varepsilon) + u_B^2(\varepsilon)}. \quad (12)$$

The expanded uncertainty is the combined standard uncertainty multiplied by a coverage factor, typically 2. This implies that the true value is presumably within the interval $\bar{\varepsilon} \pm 2u_C(\varepsilon)$ with 95 % probability. The final result of the uncertainty analysis for RLTE is expressed as

$$\varepsilon = \bar{\varepsilon} \pm 2u_C(\varepsilon), \quad (13)$$

where $\bar{\varepsilon}$ is the mean value derived from (7) and the mean values from Table 1. Upon substituting these numerical values, $\bar{\varepsilon} = 0.38 \pm 0.02$ %, i.e., the relative expanded uncertainty of RLTE is ~5.26 %.

Temperature measurements and the determination of Δt are conducted under consistent experimental conditions throughout the analysis. Consequently, this uncertainty source is invariant; it depends solely on the dilatometer properties and is independent of the sample properties. The value of Δt was transformed into an equivalent push-rod displacement Δl (see Table 2, line 5). The most significant uncertainty component arises from the scatter of ΔU values measured across a group of nominally identical samples. The scatter of ΔU, which is proportional to the scatter of RLTE, varies with the temperature, as shown in Fig. 5. Consequently, the uncertainty of RLTE is also temperature-dependent. Its values increase for t > 550 °C, where new phases emerge: meta-illite, metakaolinite, β-quartz, glass, and mullite are formed on the background of the sintering. The authors observed a similar effect when analyzing elastic modulus or electrical conductivity [29], [30].

The CLTE value at 800 °C was calculated from (4) using $\bar{\varepsilon}$ = 0.0038, and Δt = 2.5 °C yields α = 1.52 × 10^{-3} 1/K. The sensitivity coefficients for CLTE, see (10), follow from (4). Their numerical values for Δt = 2.5 °C and $\bar{\varepsilon}$ = 0.0038 are given in Table 3. The relative uncertainty of CLTE is 9.2 % at 800 °C, representing the maximum scatter of the experimental data.

When the uncertainty analysis is performed at a temperature where only ordinary thermal expansion occurs (e.g., 300 °C), the data scatter is substantially smaller (see Fig. 5). In such cases, the uncertainty of the RLTE is ~1 %, and the uncertainty of the CLTE is ~3 %.

Table 2. List of uncertainties of RLTE at room temperature and 800 °C.

	Uncertainty source	Type	Sensitivity coefficient $A(x)$	Standard uncertainty $u(x)$	$A(x)u(x)$ [-]
1	Repeatability of k at 20 °C	A	7.75 × 10^{-4} V/mm	0.002 mm/V	1.55 × 10^{-6}
2	Repeatability of l_0 at 20 °C	A	4.59 × 10^{-5} 1/mm	0.01 mm	4.59 × 10^{-5}
3	Repeatability of ΔU at 800 °C	A	–0.059 1/V	0.002 V	–1.18 × 10^{-4}
4	Repeatability of t_m transformed into Δl at 800 °C	A	4.59 × 10^{-5} 1/mm	2×10^{-4} mm	9.18 × 10^{-7}
5	The sum of A-type uncertainties $u_A(\varepsilon)$, Eq. (9)				~1.27 × 10^{-4}
6	Caliper, MAE = 0.01 mm, $U_B(l_0) = 0.01/\sqrt{3}$	B	4.59 × 10^{-5} 1/mm	5.77 × 10^{-3} mm	2.65 × 10^{-7}
7	mV-meter MAE = 1 × 10^{-5} V, $u_B(U_{LVDT}) = 1 \times 10^{-5}/\sqrt{3}$	B	–0.036 1/V	5.77 × 10^{-6} V	–2.07 × 10^{-7}
8	mV-meter MAE = 1 × 10^{-5} V, $u_B(U_{TC}) = 1 \times 10^{-5}/\sqrt{3}$	B	–0.036 1/V	5.77 × 10^{-6} V	–2.07 × 10^{-7}
9	Micrometer, r = 0.01 mm, $u_B(k) = r/\sqrt{12}$	B	4.59 × 10^{-5} 1/mm	2.9 × 10^{-3} mm	1.33 × 10^{-7}
10	Thermocouple at 800 °C	B	4.59 × 10^{-5} 1/mm	8.0 × 10^{-3} mm	3.67 × 10^{-7}
11	Temperature controller at 800 °C	B	4.59 × 10^{-5} 1/mm	1.8 × 10^{-3} mm	1.00 × 10^{-7}
12	Cold junctions	B	4.59 × 10^{-5} 1/mm	3.0 × 10^{-4} mm	1.37 × 10^{-8}
13	Inhomogeneity of temperature field at 800 °C	B	4.59 × 10^{-5} 1/mm	6.0 × 10^{-4} mm	2.75 × 10^{-8}
14	Pressure on sample	B	4.59 × 10^{-5} 1/mm	2.5 × 10^{-5} mm	1.15 × 10^{-9}
15	Sample position	B	4.59 × 10^{-5} 1/mm	2.0 × 10^{-3} mm	9.21 × 10^{-8}
16	The sum of B-type uncertainties $u_B(\varepsilon)$, Eq. (11)				5.72 × 10^{-7}
17	The combined uncertainty $u_C(\varepsilon)$, Eq. (12)				~1.27 × 10^{-4}
18	The final value of RLTE: ε = 0.0038 ± 0.0002				

Table 3. List of uncertainties of CLTE at 800 °C.

	Uncertainty source	Type	Sensitivity coefficient $A(x)$	Standard uncertainty $u(x)$	$A(x)u(x)$ [-]
1	Temperature step Δt	B	6.08×10^{-4} 1/K^2	~0.1 K	6.08×10^{-5}
2	Linear thermal expansion $(\Delta l/l_0)_s$	B	0.4 1/K	1.27×10^{-4} -	4×10^{-5}
3	The combined uncertainty $u_c(\alpha)$				7.28×10^{-5}
4	The final value of CLTE: $\alpha = (1.52 \pm 0.14) \times 10^{-3}$ 1/K				

5. Conclusions

The RLTE and CLTE of a kaolinite-based clay sample were measured using a horizontal alumina push-rod dilatometer. The dilatometer is described with respect to possible sources of uncertainty. The uncertainty analysis takes into account the homogeneity of the temperature field, the sample position, mechanical pressure on the sample, thermocouple aging and corrosion, thermocouple and temperature control, and the measurement of the LVDT output. Uncertainties associated with the measurement apparatus are also incorporated. The summation of all partial uncertainty components yields the expanded uncertainty of the thermodilatometric analysis. The uncertainty is temperature-dependent, and the expanded uncertainty reaches the highest value, ~5.26 %, at 800 °C, where transformations in sample properties generate significant data scatter. When only ordinary thermal expansion occurs, the uncertainty of the RLTE is ~1 %, and the uncertainty of the CLTE is ~3 %.

References

[1] James, J. D., Spittle, J. A., Brown, S. G. R., Evans, R. W. (2001). A review of measurement techniques for the thermal expansion coefficient of metals and alloys at elevated temperatures. *Measurement Science and Technology*, 12, R1–R15. https://doi.org/10.1088/0957-0233/12/3/201

[2] Venturelli, C., Paganelli, M. (2007). Sintering behavior of clays for the production of ceramics. *Ceramic Forum International*, 84 (5), E1-E3.

[3] Húlan, T., Trník, A., Medveď, I. (2017). Kinetics of thermal expansion of illite-based ceramics in the dehydroxylation region during heating. *Journal of Thermal Analysis and Calorimetry*, 127, 291-298. https://doi.org/10.1007/s10973-016-5873-0

[4] Ondro, T., Húlan, T., Al-Shantir, O., Csáki, Š., Václavů, T., Trník, A. (2019). Kinetic analysis of the formation of high-temperature phases in an illite-based ceramic body using thermodilatometry. *Journal of Thermal Analysis and Calorimetry*, 138, 2289-2294. https://doi.org/10.1007/s10973-019-08781-w

[5] Trník, A., Moravčíková, J., Keppert, M., Medveď, I. (2013). Investigation of sintering in electroceramics by thermodilatometry. *Science of Sintering*, 45 (1), 3-12. https://doi.org/10.2298/SOS1301003T

[6] ASTM International. (2022). *Standard test method for linear thermal expansion of solid materials with a push-rod dilatometer*. ASTM E228-22. https://store.astm.org/e0228-22.html

[7] Chmelík, F., Trník, A., Štubňa, I., Pešička, J. (2011). Creation of microcracks in porcelain during firing. *Journal of the European Ceramic Society*, 31 (13), 2205-2209. https://doi.org/10.1016/j.jeurceramsoc.2011.05.045

[8] Štubňa, I., Húlan, T., Kaljuvee, T., Vozár, L. (2018). Investigation of dynamic mechanical properties of Estonian clay Arumetsa during firing. *Applied Clay Science*, 153, 23-28. https://doi.org/10.1016/j.clay.2017.11.038

[9] Štubňa, I., Lintnerová, A., Trník, A. (2009). Mechanical properties and thermal expansion of clay ceramics measured on laboratory samples. *Industrial Ceramics*, 29 (1), 39-42.

[10] Podoba, R., Kaljuvee, T., Štubňa, I., Podobník, Ľ., Bačík, P. (2014). Research on historical bricks from a Baroque Church. *Journal of Thermal Analysis and Calorimetry*, 118, 591-595. https://doi.org/10.1007/s10973-013-3417-4

[11] Štubňa, I., Trník, A., Podoba, R., Ondruška J., Vozár, L. (2014). The influence of thermal expansion and mass loss on the Young's modulus of ceramics during firing. *International Journal of Thermophysics*, 35, 1879-1887. https://doi.org/10.1007/s10765-012-1366-y

[12] Ho, C. Y., Taylor, R. E. (eds.). (1998). *Thermal Expansion of Solids*. ASM International, ISBN 978-0871706232.

[13] Kamseu, E., Leonelli, C., Boccaccini, B. (2007). Non-contact dilatometry of hard and soft porcelain compositions. *Journal of Thermal Analysis and Calorimetry*, 88, 571-576. https://doi.org/10.1007/s10973-006-8224-8

[14] Leclerc, F. (1992). New applications of the thermodilatometry in the characterization of ceramics. *Journal of Thermal Analysis*, 38, 515-522. https://doi.org/10.1007/BF01915516

[15] Agarwal, G., Speyer, R. F., Hackenberger, W. S. (1997). A novel programmed shrinkage dilatometer for optimized sintering of powder ceramics. *Journal of Thermal Analysis*, 49, 1297-1304. https://doi.org/10.1007/BF01983687

[16] Kaiser, D., de Graaff, B., Dietrich, S., Schulze, V. (2016). A novel procedure to account for high temperature gradients in an induction dilatometer sample during rapid heating. *Thermochimica Acta*, 646, 8-15. https://doi.org/10.1016/j.tca.2016.10.014

[17] Valentich, J. (1977). Calibration of tube type dilatometers. *Journal of Thermal Analysis*, 11, 387-403. https://doi.org/10.1007/BF01903691

[18] Yamada, N., Abe, R., Okaji, M. (2001). A calibration method for measuring thermal expansion with a push-rod dilatometer. *Measurement Science and Technology*, 12, 2121-2129. https://doi.org/10.1088/0957-0233/12/12/313

[19] Liu, Y., Sommer, F., Mittemeijer, E. J. (2004). Calibration of the differential dilatometric measurement signal upon heating and cooling; thermal expansion of pure iron. *Thermochimica Acta*, 413 (1-2), 215-225. https://doi.org/10.1016/j.tca.2003.10.005

[20] Rudtsch, S., Ebert, H. P., Hemberger, F., Barth, G., Brandt, R., Groß, U., Hohenauer, W., Jaenicke-Roessler, K., Kaschnitz, E., Pfaff, E., Pößnecker, W., Pottlacher, G., Rhode. M., Wilthan, B. (2005). Intercomparison between thermophysical property measurements on an austenitic stainless steel. *International Journal of Thermophysics*, 26, 855-867. https://doi.org/10.1007/s10765-005-5582-6

[21] Henderson, J. B., Emmerich, W.-D., Wassmer, E. (1987). A method for the temperature calibration of pushrod dilatometers. *Journal of Thermal Analysis*, 32, 1905-1913. https://doi.org/10.1007/BF01913983

[22] Raz, U., Girsperger, S., Thomson, A. B. (2002). Thermal expansion, compressibility and volumetric changes of quartz obtained by single crystal dilatometry to 700 degrees C and 3.5 kilobar (0.35 GPa). *Swiss Journal of Geosciences Supplement*, 82 (3), 561-574. https://doi.org/10.3929/ETHZ-A-004392716

[23] Jay, A. H. (1933). The thermal expansion of quartz by X-ray measurements. *Proceedings of the Royal Society A*, 142 (846), 237-247. https://doi.org/10.1098/rspa.1933.0165

[24] Sorrell, C. A., Anderson, H. U., Ackermann, R. J. (1974). Thermal expansion and the high–low transformation in quartz. II. Dilatometric studies. *Journal of Applied Crystallography*, 7 (5), 468-473. https://doi.org/10.1107/S0021889874010223

[25] Skinner, B. J. (1966). Thermal expansion. In *Handbook of Physical Constants*. Geological Society of America, 75-96. https://doi.org/10.1130/MEM97-p75

[26] Pryanishnikov, V. P. (1971). *Sistema kremnezema [The System of Silica]*. Leningrad, USSR: Stroyizdat. (in Russian)

[27] ISO. (2008). *Uncertainty of measurement - Part 3: Guide to the expression of uncertainty in measurement (GUM:1995)*. ISO/IEC Guide 98-3:2008. https://www.iso.org/standard/50461.html

[28] Deutsches Institut für Normung. (2005). *Bestimmung der thermischen Längenänderung fester Körper - Teil 1: Grundlagen [Determination of the thermal expansion of solids - Part 1: Basic rules]*. DIN 51045-1. https://dx.doi.org/10.31030/9636919

[29] Štubňa, I., Húlan, T., Trník, A., Vozár, L. (2018). Uncertainty in the determination of Young's modulus of ceramics using the impulse excitation technique at elevated temperature. *Acta Acustica*, 104 (2), 269-276. https://doi.org/10.3813/AAA.919169

[30] Štubňa, I., Trnovcová, V., Vozár, L., Csáki, Š. (2015). Uncertainty of the measurement of DC conductivity of ceramics at elevated temperatures. *Journal of Electrical Engineering*, 66 (1), 34-39. https://doi.org/10.1515/jee-2015-0005

Received April 23, 2026
Accepted September 21, 2026